Temperature Dependence of Electron Mobility in Uniaxial Strained nMOSFETs

Wookyung Sun and Hyungsoon Shin

***Abstract*—The temperature dependence of strain-enhanced electron mobility in nMOSFETs is investigated by using a self-consistent Schrödinger-Poisson solver. The calculated results suggest that vertical compressive stress is more efficient to maintain the strain-enhanced electron mobility than longitudinal tensile stress in high temperature condition.**

***Index Terms*—Electron mobility, stress, strain, intravalley phonon mobility, intervalley phonon mobility, temperature**

I. INTRODUCTION

As the device dimension shrinks, the enhancement of carrier mobility by strain has been investigated to improve device performance. The strain changes the electronic band structure resulting in the change of carrier mobility [1-5]. While the electrostatics of strained MOSFETs has been studied, several research groups have reported the mobility characteristic in strained MOSFETs [1, 6] or in unstrained MOSFETs [7, 8]. It is also reported that the intervalley phonon scattering is required to accurately explain the behavior of inversion layer mobility in both strained and unstrained Si MOSFETs [9]. Furthermore, Si devices in VLSI logic chips have been used in high temperature environments recently. The mobility of carrier is closely related to the temperature. Thus, it is important to know the characteristic of strain-induced electron mobility enhancement in high temperature condition. However, there is very little information on the relation between temperature and uniaxial stress-induced electron mobility enhancement [10, 11].

The aim of this paper is to explain the temperature dependence of uniaxial strain-induced electron mobility in nMOSFETs. Among several stress conditions, we focus on the longitudinal tensile (L-T) and vertical compressive (V-C) uniaxial stress because these stresses are widely used as process-induced uniaxial stress to improve the electron mobility.

II. MOBILITY SIMULATION

We calculated the wave functions using our Schrödinger-Poisson solver. In addition, the phonon scattering mobility (μ_{ph}), coulomb mobility (μ_{coul}) and surface roughness mobility (μ_{sr}) on the (100)/<110> Si surfaces were also calculated through our solver. To consider the physical mechanism of mobility enhancement in strained nMOSFETs, we take the intravalley and intervalley phonon scattering into account [6, 8]. The traditional theory of intravalley and intervalley phonon scattering has already been developed and expressions for the momentum relaxation rate have been obtained. The momentum relaxation rate by intravalley acoustic phonons (τ^i_{intra}) from the i th subband to the j th subband is given by

$$\frac{1}{\tau^i_{intra}(E)} = \sum_j \frac{n_i^{ac} m_{d,j} D^2_{ac,eff} k_B T}{\hbar^3 \rho s_l^2} F_{i,j} U(E - E_j), \tag{1}$$

$$F_{i,j} = \int_{-\infty}^{+\infty} |\xi_i(z)|^2 \left|\xi_j(z)\right|^2 dz \quad , \tag{2}$$

Manuscript received Aug. 10, 2013; accepted Feb. 9, 2014
Department of Electronic Engineering, Ewha Womans University
E-mail : hsshin@ewha.ac.kr

where n_i^{ac} is the degeneracy of the valley with respect to intravalley scattering, $m_{d,j}$ is the density-of-state effective mass of electrons at the j th subband, $D_{ac,eff}$ is the effective intravalley deformation potential for acoustic phonon scattering, ρ is the mass density of the crystal, s_l is the longitudinal sound velocity, and $U(x)$ is the Heaviside step function. $F_{i,j}$ is the form factor determined by the wave functions of the i th and the j th subbands [6].

The momentum relaxation rate for intervalley phonon scattering (τ^i_{inter}) from the i th subband to the j th subband is given by

$$\frac{1}{\tau^i_{inter}(E)} = \sum_j \left\{ \sum_k^{\{f,g\}} \frac{n_{ij}^{f,g} m_{d,j} D^2_{k,eff}}{\hbar \rho E_k} F_{i,j} \left(N_k + \frac{1}{2} \pm \frac{1}{2} \right) \cdot \frac{1 - f(E \mp E_k)}{1 - f(E)} U(E \mp E_k - E_j) \right\} \quad , \tag{3}$$

where k is the index of phonons and $n_{ij}^{f,g}$ is the degeneracy of the valley j undergoing an intervalley transition from valley i to valley j, $D_{k,eff}$ is the effective deformation potential of the k th intervalley phonon, E_k is the energy of the k th intervalley phonon, N_k is the Bose-Einstein distribution function, and $f(E)$ is the Fermi-Dirac distribution function. In (3), f and g are the type of intervalley scattering. The upper or lower sign must be taken for the process of emission and absorption of phonons, respectively [6]. The physical parameters used in equations are listed in Table 1. Also, Fig. 1 represents the schematic of phonon scattering for (100) orientation in the 3-D E-k band structures. 'E_0' is the lowest energy level of $\Delta 2$ valley. Intravalley phonon scattering occurs in each valley. 'f type' intervalley phonon scattering occurs within $\Delta 2$ and $\Delta 4$ valleys and 'g type' intervalley phonon scattering occurs within each $\Delta 2$ or $\Delta 4$ valleys.

The total relaxation rate (τ^i) with the energy E for i th subband is given by

$$\frac{1}{\tau^i(E)} = \frac{1}{\tau^i_{intra}(E)} + \frac{1}{\tau^i_{inter}(E)} \quad . \tag{4}$$

The electron mobility in the i th subband (μ^i) and phonon scattering mobility (μ_{ph}) are given by

$$\mu^i = \frac{q \int_{E_i}^{\infty} (E - E_i)\, \tau^i(E)(-\partial f / \partial E) dE}{m_{c,i} \int_{E_i}^{\infty} (E - E_i)(-\partial f / \partial E) dE}, \tag{5}$$

Table 1. Physical parameters used in this paper

Symbol	Value	Definition
m_0	9.11×10^{-31} kg	free electron mass
ρ	2329 kg/m^3	crystal mass density
s_l	9037 m/s	longitudinal sound velocity
$m_{c\,\Delta 2}$	0.19 m_0	conductivity mass of $\Delta 2$
$m_{c\,\Delta 4}$	0.315 m_0	conductivity mass of $\Delta 4$
$m_{d\,\Delta 2}$	0.19 m_0	density of state mass of $\Delta 2$
$m_{d\,\Delta 4}$	0.417 m_0	density of state mass of $\Delta 4$
$m_{z\,\Delta 2}$	0.916 m_0	quantization mass of $\Delta 2$
$m_{z\,\Delta 4}$	0.19 m_0	quantization mass of $\Delta 4$
D_{ac}	12 eV	intravalley deformation potential at $E_{\text{eff}} = 0.1$MV/cm
D_k	8×10^8 eV/cm	intervalley deformation potential at $E_{\text{eff}} = 0.1$MV/cm
E_k	59 meV 63 meV	energy of f type intervalley energy of g type intervalley
$n_{\Delta 2}^{ac}$ $n_{\Delta 4}^{ac}$	1 1	degeneracy number of each valley for intravalley scattering
$n^g_{\Delta 2\,\Delta 2}$ $n^f_{\Delta 2\,\Delta 4}$ $n^g_{\Delta 4\,\Delta 4}$ $n^f_{\Delta 4\,\Delta 2}$ $n^f_{\Delta 4\,\Delta 4}$	1 4 1 2 2	degeneracy number of each valley for intervalley scattering

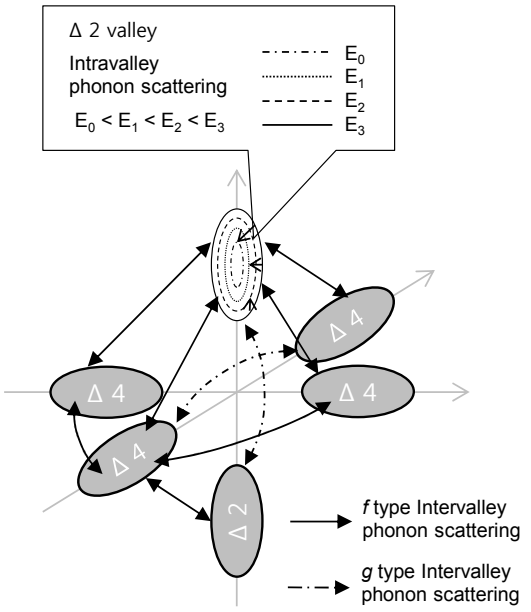

Fig. 1. Schematic of phonon scattering for (100) orientation in the 3-D E-k energy-band structures.

$$\mu_{ph} = \frac{\sum_i \left(\mu^i N_i \right)}{N_S} \quad , \tag{6}$$

where $m_{c,i}$ is the conductivity mass of i th subband. In the equation above, N_i is the carrier density of the i th subband, and N_s is the total carrier density. We also calculate μ_{sr} and μ_{coul} using the equation described in [7]

and [12].

In order to more accurately calculate the μ_{ph}, we use the concept of effective deformation potential which means the deformation potential is changed by effective electric field (E_{eff}). For silicon, intervalley phonon energy (E_k) depends on *f* type and *g* type scattering mechanisms and we used E_k parameter set proposed by Ferry [13]. In case of intravalley deformation potential (D_{ac}), various D_{ac} parameter sets are usually used to represent the experimental mobility. In addition, some of them suggest that the effective deformation potential should be dependent on surface-field [14, 15]. So, in this work, $D_{ac,eff}$ and $D_{k,eff}$ are modeled to realize effective deformation potential, as

$$D_{ac,eff}(E_{eff}) = A + B(E_{eff})^{0.3} \quad , \tag{7}$$

$$D_{k,eff}(E_{eff}) = D_k \cdot \frac{D_{ac,eff}(E_{eff})}{D_{ac}} \quad , \tag{8}$$

where D_{ac} and D_k are deformation potentials at E_{eff} = 0.1MV/cm, E_{eff} is the effective electric field, and 0.3 is theoretically equal to electric field dependence of carrier mobility on a (100) surface [16]. The fitting parameters A and B are determined from two limits that $D_{ac,eff}$ at E_{eff} = 0.1MV/cm is 12eV and $D_{ac,eff}$ at 1MV/cm is 18eV, and we used A = 9.34, B = 0.12 for a (100) orientation.

Analytical expressions for the strain-induced valley splitting and effective mass changes of the (110)/<110> have been reported in [17]. However, the stress effect of valley and the effective mass in the (100)/<110> have not been explained. So, we derived analytical expressions for the stress-induced changes of the conduction band minima and effective mass.

According to the theory of elasticity, the general relation between stress and strain tensors is described by a matrix equation [18]. The strain-induced energy shifts are given by [17, 19]

$$E_{\Delta i,0} = \Xi_d(\varepsilon_{xx} + \varepsilon_{yy} + \varepsilon_{zz}) + \Xi_u \varepsilon_{ii} + E^{shear}_{\Delta i,0} \ , \ i = x, y, z \tag{9}$$

with

$$E^{shear}_{\Delta x,0} = -\frac{\Theta}{4k^2}\varepsilon^2_{yz} \tag{10}$$

$$E^{shear}_{\Delta y,0} = -\frac{\Theta}{4k^2}\varepsilon^2_{xz}$$

$$E^{shear}_{\Delta z,0} = -\frac{\Theta}{4k^2}\varepsilon^2_{xy} \quad ,$$

where ε_{xx}, ε_{yy}, and ε_{zz} are the normal-strain components and ε_{yz}, ε_{xz}, and ε_{xy} are the shear-strain components. The numerical values for (9) and (10) are reported in Table 2. We also obtained the strain induced energy shift in the (100)/<110> by substituting the components of the strain tensor and the numerical parameters reported in Table 2:

$$\begin{aligned} E_{\Delta 2,0} &= \Xi_d(\varepsilon_{xx} + \varepsilon_{yy} + \varepsilon_{zz}) + \Xi_u \varepsilon_{zz} + E^{shear}_{\Delta z,0} \\ &= -17.28(T_L + T_W) + 74.97T_V - 3.62(-T_L + T_W)^2 \end{aligned} \tag{11}$$

$$\begin{aligned} E_{\Delta 4,0} &= \Xi_d(\varepsilon_{xx} + \varepsilon_{yy} + \varepsilon_{zz}) + \Xi_u \varepsilon_{xx} \\ &= \Xi_d(\varepsilon_{xx} + \varepsilon_{yy} + \varepsilon_{zz}) + \Xi_u \varepsilon_{yy} \\ &= 28.85(T_L + T_W) - 17.28T_V \end{aligned} \tag{12}$$

where $E_{\Delta 2,0}$ and $E_{\Delta 4,0}$ is the strain induced energy shift for Δ2 and Δ4 valley. T_L, T_W, and T_V are the stress components in the gate length, gate width, and gate vertical direction. They are in gigapascal. The masses of Δ2 valley are changed by the shear strain component in the (100)/<110>, and it is given by [17, 19]

$$\begin{aligned} m_{\Delta 2,c} &= m_t\left(1 + \frac{|\eta|}{k}\varepsilon_{xy}\right)^{-1} \\ m_{\Delta 2,q} &= m_l\left(1 - \frac{1}{k^2}\varepsilon_{xy}{}^2\right)^{-1} \\ m_{\Delta 2,d} &= m_t\left(1 - \frac{|\eta|}{k}\varepsilon_{xy}\right)^{-1} \end{aligned} \tag{13}$$

where $m_{\Delta 2,c}$, $m_{\Delta 2,q}$, and $m_{\Delta 2,d}$ are the conductivity, quantization, and density of state mass of Δ2 valley,

Table 2. Physical parameters used in this paper

Symbol	Value	Definition
m_l	0.916 m_0	longitudinal effective mass
m_t	0.19 m_0	transverse effective mass
Ξ_u	9.29 eV	uniaxial deformation potential
Ξ_d	1.1 eV	dilatation deformation potential
Θ	0.53 eV	k·p model parameter
η	-0.809	
k	0.0189	

respectively. The physical parameters used in (13) are listed in Table 2.

The calculated electron mobility of unstrained Si agrees well with experimental data. In Figs. 2 and 3, the calculated total mobility in the (100)/<110> is compared with the experimental data in [16] for various temperatures and N_{sub}. As can be seen, our calculation results describe the total electron mobility with temperature and N_{sub} in the high E_{eff} well.

Fig. 4 is the strain dependence of μ_{eff} enhancement induced by uniaxial longitudinal and transverse tensile stress, and our numerically calculated results show good agreement with experimental data taken from [20]. As can be shown in Figs. 2-4, our numerically calculated mobility shows good agreement with the experimental data. Therefore, it is reasonable that we use our numerically calculated results to predict the strain-induced mobility enhancement for various cases.

III. TEMPERATURE DEPENDENCE ON STRESS

Fig. 5 shows the μ_{eff} as a function of temperature under uniaxial stress. A comparison with experimental data under unstrain condition taken from [10] is also shown in Fig. 5. The magnitude of L-T (longitudinal tensile) stress and V-C (vertical compressive) stress is 0.5 and 1 GPa. At 0.5 GPa, the temperature dependence of μ_{eff} under L-T and V-C stress is similar to that under unstrain condition. However, the slope of μ_{eff} under V-C stress in 1GPa differs from others. To examine the origin of μ_{eff}

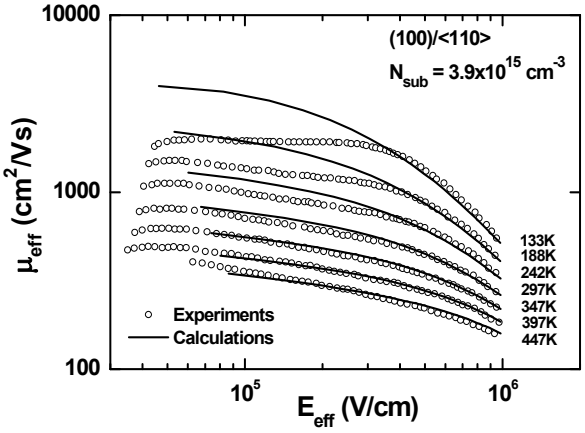

Fig. 2. E_{eff} dependence of the total electron mobility for various temperatures. The symbols represent the experimental data from [16]. The solid lines represent the numerically calculated total mobility.

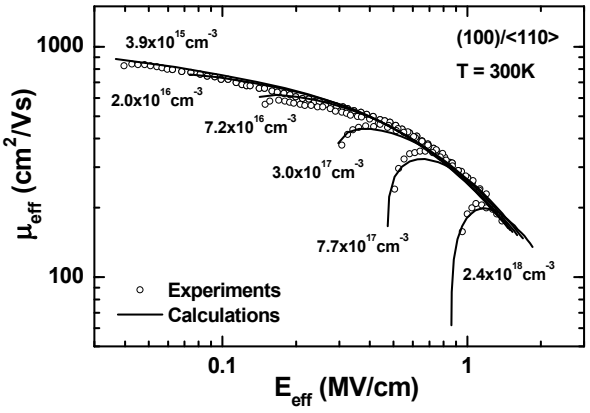

Fig. 3. E_{eff} dependence of the total electron mobility for various N_{sub}. The symbols represent the experimental data from [16]. The solid lines represent the numerically calculated total mobility.

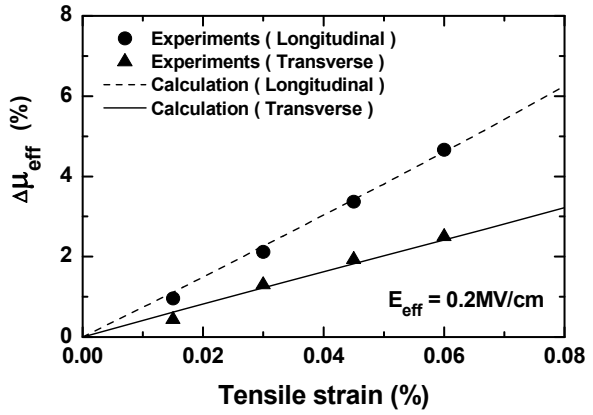

Fig. 4. Strain dependence of the μ_{eff} enhancement induced by uniaxial longitudinal and transverse tensile strain. The symbols represent the experimental data from [20]. The solid and dash lines represent numerically calculated results using the effective deformation potential.

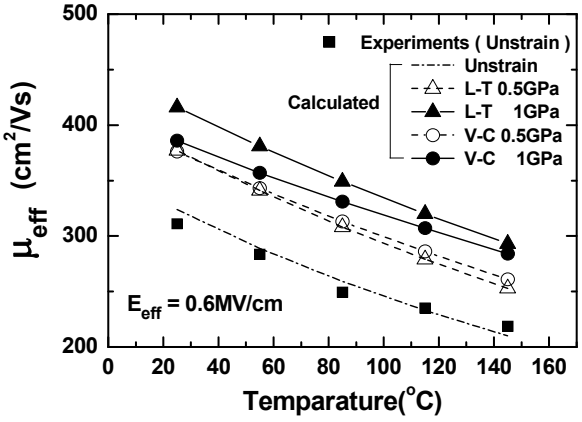

Fig. 5. The temperature dependence of the μ_{eff} for various stress conditions. The square symbol represents the experimental data from [10]. L-T means the longitudinal tensile stress and V-C is the vertical compressive stress.

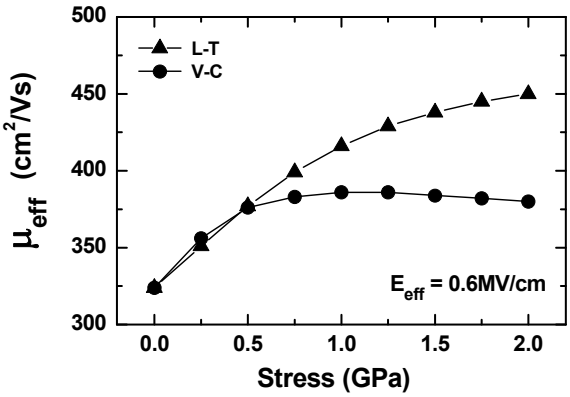

Fig. 6. The stress dependence of μ_{eff} for L-T (longitudinal tensile) and V-C (vertical compressive) stress condition.

difference between L-T and V-C stress in 1 GPa at room temperature, we calculate the stress dependence of μ_{eff}. In Fig. 6, L-T and V-C stress show different stress dependence. It is important to notice that the μ_{eff} is increased continuously by L-T stress, while the μ_{eff} under V-C stress is saturated at 0.5 GPa. Therefore, the contrast of stress dependence between them is the main cause of strain-induced mobility enhancement at room temperature. The reason for this difference between L-T and V-C stress is the effective conductivity mass (m_c) of Δ2 valley. In other words, m_c of Δ2 valley is changed by L-T stress, whereas V-C stress does not change the m_c of Δ2 valley.

In Fig. 5, another important property is that temperature-induced mobility degradation under V-C stress in 1 GPa is smaller than that under L-T stress at high temperature. To investigate the cause of mobility enhancement, we calculate the occupancy of each subband. In case of (100)/<110>, Δ2 valleys is more important than Δ4 valleys because Δ2 valley is unprimed valley and m_c of Δ2 valley is smaller than Δ4 valley. Fig. 7 is the calculated occupancy of Δ2 valleys for various stress conditions as a function of temperature. The occupancy of Δ2 valleys in L-T stress is smaller, although the μ_{eff} induced by L-T stress is larger than V-C stress, since L-T stress decreases the m_c of Δ2 valley. The μ_{eff} is influenced by both the occupancy of subbands and m_c, however m_c is not changed by temperature. Therefore, we may conclude that temperature dependency of μ_{eff} induced by strain, as shown in Fig. 5, is mainly due to the relative occupancy of subbands.

To examine these occupancy characteristics, we confirmed the bottom subband energy of each valley and Fermi-Dirac (FD) distribution at 25℃ and 145℃. Fig. 8 shows the calculated conduction band energy (E_C) and Fermi-Dirac distribution. E_0 represents the bottom subband energy of Δ2 valley and E'_0 is the bottom subband energy of Δ4 valley. In Fig. 7, occupancy of Δ2 valleys decreased significantly as temperature increased in L-T stress. It is due to the substantial increase of FD of Δ4 valley at high temperature as shown Fig. 8. On the contrary, the temperature dependency of FD is small in

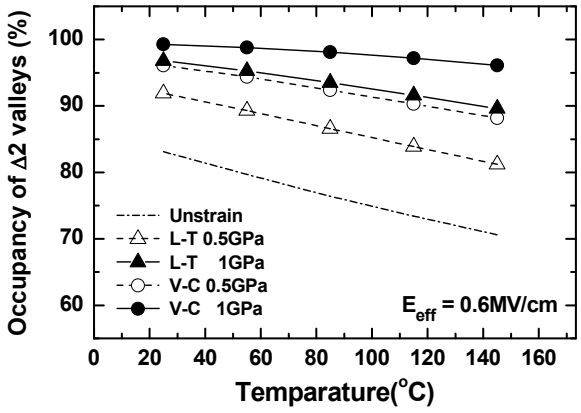

Fig. 7. Calculated occupancy of Δ2 valleys for various stress conditions as a function of temperature. L-T means the longitudinal tensile stress and V-C is the vertical compressive stress.

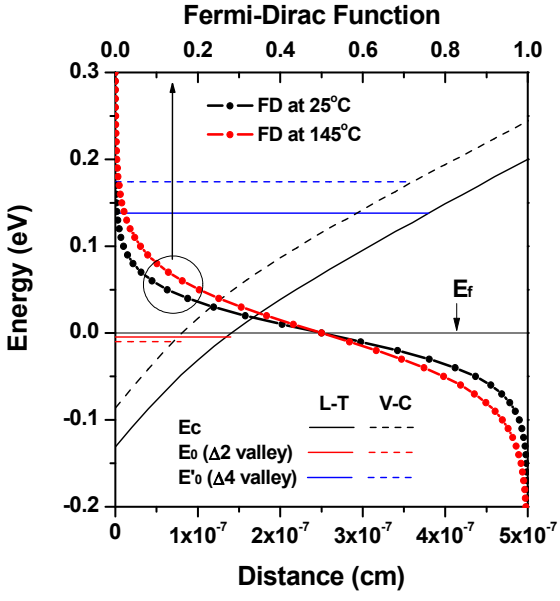

Fig. 8. Calculated conduction band energy (E_C) and Fermi-Dirac distribution. E_0 represents the bottom subband energy of Δ2 valley and E'_0 is the bottom subband energy of Δ4 valley. The solid and dash lines represent L-T and V-C stress condition, respectively.

case of V-C stress because the bottom subband energy of Δ4 valley is higher than L-T stress. Therefore the occupancy of Δ2 valleys induced by V-C stress shows mush less temperature dependency than L-T stress. It means that V-C stress is more effective than L-T stress to preserve the strain effect for electron mobility at high temperature. In other words, V-C stress is more efficient to maintain the strain enhanced electron mobility enhancement at high temperature condition.

IV. CONCLUSIONS

In order to investigate the strain-induced electron mobility characteristic, we calculate the mobility for various temperatures using the Schrödinger-Poisson solver and consider the intervalley and intravalley phonon scattering mobility simultaneously in strained Si. We also derived analytical expressions for the stress-induced changes of the conduction band minima and effective mass in the (100)/<110>. It is found that temperature dependency of mobility induced by strain is mainly due to the relative occupancy of subbands. Conclusively, our calculation results propose that the vertical compressive stress (V-C) is the more effective stress engineering to maintain the strain-enhanced electron mobility at high temperature rather than longitudinal tensile stress (L-T).

ACKNOWLEDGMENTS

This research was supported by Basic Science Research Program through the National Research Foundation of Korea (NRF) funded by the Ministry of Education, Science and Technology (No. 2010-0007016).

REFERENCES

[1] M. V. Fischetti, F. Gámiz, and W. Hänsch, "On the enhanced electron mobility in strained-silicon inversion layers," *J. Appl. Phys.*, vol. 92, no. 12, pp. 7320–7324, Dec. 2002.

[2] S. E. Thompson, M. Armstrong, C. Auth, S. Cea, R. Chau, G. Glass, T. Hoffman, J. Klaus, Z. Ma, B. Mcintyre, A. Murthy, B. Obradovic, L. Shifren, S. Sivakumar, S. Tyagi, T. Ghani, K. Mistry, M. Bohr, and Y. El-Mansy, "A logic nanotechnology featuring strained-silicon," *IEEE Electron Device Lett.*, vol. 25, no. 4, pp. 191–193, Apr. 2004.

[3] K. -W. Ang, K. –J. Chui, C. –H. Tung, N. Balasubramanian, M. –Fu. Li, G. S. Samudra, and Y. –C. Yeo, "Enhanced strain effects in 25-nm gate-length thin-body nMOSFETs with silicon-carbon source/drain and tensile-stress liner," *IEEE Electron Device Lett.*, vol. 28, no. 4, pp. 301–304, Apr. 2007.

[4] K. Uchida, M. Saitoh, and S. Kobayashi, "Carrier transport and stress engineering in advanced nanoscale transistors from (100) and (110) transistors to carbon nanotube FETs and beyond," in *IEDM Tech. Dig.,* 2008, pp. 1–4.

[5] S. Takagi, T. Irisawa, T. Tezuka, T. Numata, S. Nakaharai, N. Hirashita, Y. Moriyama, K. Usuda, E. Toyoda, S. Dissanayake, M. Shichijo, R. Nakane, S. Sugahara, M. Takenaka, and N. Sugiyama, "Carrier-transport-enhanced channel CMOS for improved power consumption and performance," *IEEE Trans. Electron Devices*, vol. 55, no. 1, pp. 21–39, Jan. 2008.

[6] S. Takagi, J. L. Hoyt, J. J. Welser, and J. F. Gibbons, "Comparative study of phonon-limited mobility of two-dimensional electrons in strained and unstrained Si metal-oxide-semiconductor field-effect transistors," *J. Appl. Phys.*, vol. 80, no. 3, pp. 1567–1577, Aug. 1996.

[7] K. Masaki, C. Hamaguchi, K. Taniguchi, and M. Iwase, "Electron mobility in Si inversion layers," *Japan. J. Appl. Phys.*, vol. 28, no. 10, pp. 1856–1863, Oct. 1989.

[8] Y. Omura, T. Yamamura, and S. Sato, "Low-temperature behavior of phonon-limited electron mobility of sub-10-nm thick silicon-on-insulator metal-oxide-semiconductor field-effect transistor with (001) and (111) Si Surface channels," *Japan. J. Appl. Phys.*, vol. 48, pp. 071204–1, Jul. 2009.

[9] S. Takagi, J. L. Hoyt, J. J. Welser, and J. F. Gibbons, "Importance of inter-valley phonon scattering on mobility enhancement in strained Si MOSFETs," in *Proc. Int. Conf. SISPAD Tech.,* 1996, pp. 5–6.

[10] T. -S. Chang, T. Y. Lu, and T. –S. Chao, "Temperature dependence of electron mobility on strained nMOSFETs fabricated by strain-gate engineering," *IEEE Electron Device Lett.*, vol. 33,

no. 7, pp. 931–933, Jul. 2012.

[11] P. C. Huang, S. L. Wu, S. J. Chang, C. W. Kuo, C. Y. Chang, Y. T. Huang, Y. C. Cheng and O. Cheng, "Temperature dependence of electrical characteristics of strained nMOSFETs using stress memorization technique," *IEEE Electron Device Lett.*, vol. 32, no. 7, pp. 835–837, Jul. 2011.

[12] H. Shin, G. M. Yeric, A. F. Tasch and C. M. Maziar, "Physicaly-based models for effective mobility and local-field mobility of electrons in MOS inversion layers," *Solid-State Electronics,* vol. 34, pp. 545–552, Jun. 1991.

[13] D. K. Ferry, *Semiconductors*, 1st ed., Macmillan, N.Y, 2000, pp. 223-225.

[14] C. –Y. Wu, and G. Thomas, "Two-dimensional electron-lattice scattering in thermally oxidized silicon surface-inversion layers," *Phy. Rev. B*, vol. 9, pp. 1724–1732, Feb. 1974.

[15] R. Shah, and M. M. Souza, "Semi-empirical phonon scattering model," in *Proc. World Congress on Engineering*, 2009.

[16] S. Takagi, A. Toriumi, M. Iwase, and H. Tango, "On the universality of inversionlayer mobility in Si MOSFET's: Part I – Effects of substrate impurity concentration," *IEEE Trans. Electron Devices*, vol. 41, no. 12, pp. 2357–2362, Dec. 1994.

[17] N. Serra, and D. Esseni, "Mobility enhancement in strained n-FinFETs: Basic insight and stress engineering," *IEEE Trans. Electron Devices*, vol. 57, no. 2, pp. 482–490, Feb. 2010.

[18] M. -H. Bao, *Micro Mechanical Transducers,*1st ed., Elsevier Science, 2000, pp. 30-31.

[19] E. Ungersboeck, S. Dhar, G. Karlowatz, V. Sverdlov, H. Kosina, and S. Selberherr, "The effect of general strain on the band structure and electron mobility of silicon," *IEEE Trans. Electron Devices*, vol. 54, no. 9, pp. 2183–2190, Sep. 2007.

[20] K. Uchida, T. Krishnamohan, K. C. Saraswat, and Y. Nishi, "Physical mechanisms of electron mobility enhancement in uniaxial stressed MOSFETs and impact of uniaxial stress engineering in ballistic regime," in *IEDM Tech. Dig.,* 2005, pp. 1–4.

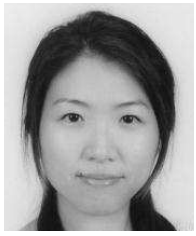

Wookyung Sun received the B.S. and M.S. degrees in electronics engineering from Ewha Womans University, Seoul, Korea, in 1999 and 2001, respectively. From 2001 to 2009, she was with Hynix semiconductor, Ltd., in Korea, where she was engaged in research on the development of DRAM memory. She is currently working toward the Ph.D. degree in electronics engineering from Ewha Womans University, Seoul, Korea. Her research interest includes the 3-D multi gate devices, strain effect based on Si MOSFETs, and TFT devices.

Hyungsoon Shin received the B.S. degree in electronics engineering from Seoul National University, Seoul, Korea, in 1982, and the M.S. and Ph.D. degrees in electrical engineering from the University of Texas at Austin, Austin, in 1984 and 1990, respectively. From 1990 to 1994, he was with LG Semicon Company, Ltd., in Korea, where he was engaged in research on the development of DRAM, SRAM, and Flash memory. Since 1995, he has been with the Department of Electronics Engineering, EWHA Womans University, Seoul. His current research interests include new processes, devices, and circuit developments and modeling based on Si, both for high-density memory and RF ICs.